# Calculation of the intersubband absorption strength in ellipsoidal-valley quantum wells

E. R. Brown and S. J. Eglash
*Lincoln Laboratory, Massachusetts Institute of Technology, P.O. Box 73, Lexington, Massachusetts 02173-0073*
(Received 19 September 1989; revised manuscript received 18 December 1989)

A new calculation is made of the quantum-well intersubband absorption by electrons that occupy valleys with ellipsoidal constant-energy surfaces. Application of the results to the special case of spherical-valley materials yields excellent agreement with recent experimental results for GaAs quantum wells. According to the calculation, strong intersubband absorption is exhibited by ellipsoidal-valley quantum wells in indirect-band-gap $Al_xGa_{1-x}As$ and $Al_xGa_{1-x}Sb$ alloys, and both materials have the advantage over GaAs of being able to absorb light incident normal to the quantum-well plane. For a wavelength of 10 $\mu$m, sheet concentration of $7.6\times10^{11}$ cm$^{-2}$, and a linewidth of 11 meV, the calculated fractional absorptions for normally incident light on a (111) $Al_{0.5}Ga_{0.5}As$ and (100) $Al_{0.3}Ga_{0.7}Sb$ quantum well are 0.000 73 and 0.0022, respectively, independent of the azimuthal angle of polarization. The absorption is stronger for $Al_xGa_{1-x}Sb$ than for $Al_xGa_{1-x}As$ because the ellipsoid eccentricity is greater for $L$ valleys than for $X$ valleys in these materials.

## I. INTRODUCTION

There is considerable interest in using the intersubband transitions in semiconductor quantum wells[1] as the basis for long-wavelength infrared detectors[2] or emitters.[3] The primary advantages of the quantum-well approach are: (1) the ability to vary the well width to adjust the transition energies and, therefore, the wavelength response of the detector or emitter, and (2) the ability to utilize semiconductor planar technology, which will facilitate the fabrication of device arrays. At present the most developed quantum-well material system is (100) $GaAs/Al_xGa_{1-x}As$, in which the conduction electrons occupy a valley with spherical constant-energy surfaces. A major shortcoming of this system for detector applications is that intersubband transitions require the incident photon polarization to be perpendicular to the plane of the well. For many practical devices it is much more convenient to absorb photons polarized parallel to the well, i.e., an incident photon flux that is normal to the wafer surface. The limitation on polarization does not necessarily apply to quantum wells in which the electrons occupy valleys with ellipsoidal constant-energy surfaces (ellipsoidal valleys). This fact was realized during studies of quantized inversion layers in Si metal-oxide-semiconductor field-effect transistors (MOSFET's),[4] and has been observed in several different experiments.[5–8] Recently, ellipsoidal-valley materials were proposed for quantum wells, and calculations were presented for the $Si_xGe_{1-x}$ system.[9]

In this paper we carry out a new calculation of the quantum-well intersubband absorption by electrons in ellipsoidal valleys. Our theoretical derivation follows directly from the effective-mass theorem, and is similar in many ways to the treatments of electron cyclotron resonance in bulk Si and Ge.[10] We find it possible for an ellipsoidal-valley quantum well to strongly absorb incident light polarized in the plane of the well. Specifically, an ellipsoidal valley of electrons can contribute to such absorption if none of its principal axes (projected onto the crystal coordinates) is collinear with the incident field. The same qualitative conclusion was drawn by Yi and Quinn[11] in their study of Si MOSFET's, and by Yang *et al.*[9] in their analysis of Si/Ge quantum wells. However, we find the strength of absorption to be considerably greater than calculated in the latter work for the two technologically important examples of (111)-oriented wells made of Si-like materials and (100)-oriented wells made of Ge-like materials. Furthermore, we confirm for these cases that the absorption is independent of the azimuthal angle of the incident electric field, as expected on symmetry grounds. This is an important advantage in applying quantum wells as infrared detectors of unpolarized radiation.

## II. PERTURBATION HAMILTONIAN

The energy dispersion relation for electrons in an ellipsoidal valley is

$$E(\mathbf{k})=E(\mathbf{k}_0)+\frac{1}{2}\sum_{m,n=1}^{3}(k_m-k_{0m})\frac{\partial^2 E(\mathbf{k}_0)}{\partial k_m\,\partial k_n}(k_n-k_{0n})\ , \tag{1}$$

where $k_{0n}$ is the $n$th component of the vector $\mathbf{k}_0$ in momentum space that locates the center of the ellipsoid. The set of values $\partial^2 E(\mathbf{k}_0)/\partial k_m\,\partial k_n$ defines a tensor that is real and symmetric, and thus can be diagonalized along any one of the three principal axes of the ellipsoid. In the presence of an applied electromagnetic field, the electron momentum and the vector potential are coupled in a manner described by the Luttinger-Kohn corollary to the

 

effective-mass theorem,[12]

$$E(\mathbf{k}_0+\mathbf{P}/\hbar-e\,\mathbf{A}/\hbar c)F(\mathbf{r})=\varepsilon F(\mathbf{r})\ , \tag{2}$$

where $\mathbf{A}$ is the vector potential, $F(\mathbf{r})$ is a slowly varying (over a unit cell) envelope function, $\mathbf{P}$ is the canonical momentum operator, and $\varepsilon$ is the total-energy eigenvalue. Using the functional form for $E(\mathbf{k})$ given by Eq. (1), we obtain

$$\left[\frac{1}{2}\sum_{m,n=1}^{3}\left[P_m-\frac{eA_m}{c}\right]w_{mn}\left[P_n-\frac{eA_n}{c}\right]\right]F(\mathbf{r})=\varepsilon F(\mathbf{r})\ , \tag{3}$$

where $w_{mn}$ is the reciprocal effective-mass tensor component equal to $(\hbar)^{-2}\partial^2E(\mathbf{k}_0)/\partial k_m\,\partial k_n$, and $\varepsilon$ is now measured relative to $E(\mathbf{k}_0)$. This expression can be expanded to yield a total Hamiltonian of the form $H=H_0+H_P$, where $H_0=\frac{1}{2}\sum_{m,n}w_{mn}P_mP_n$. The perturbation term is given by

$$H_P=-\frac{e}{c}\sum_{m,n=1}^{3}\frac{w_{mn}}{2}\left[[A_m,P_n]_+-\frac{e}{c}A_mA_n\right]\ , \tag{4}$$

where $[\ ,\ ]_+$ denotes anticommutation, and the symmetry of the reciprocal effective-mass tensor (i.e., $w_{mn}=w_{nm}$) has been utilized. Photon absorption is analyzed with a vector potential in the form of a harmonic plane wave,

$$\mathbf{A}=\sum_{n=1}^{3}A_n\mathbf{e}_n\exp[i(\boldsymbol{\beta}\cdot\mathbf{r}-\omega t)]+\text{c.c.}\ , \tag{5}$$

where $\mathbf{A}\cdot\boldsymbol{\beta}=0$, $\boldsymbol{\beta}$ is the propagation vector, and $\mathbf{e}_n$ is a unit vector. The gauge is chosen (without loss of generality) so that the scalar potential $\phi=0$. We assume $|\mathbf{A}|$ to be small enough that terms of order $A_n^2$ can be ignored in Eq. (4).

## III. UNPERTURBED ENVELOPE FUNCTIONS

We apply this formalism to the problem of intersubband transitions in a quantum well. The first task is to determine the form of the unperturbed wave functions by solving the following Schrödinger equation:

$$\left[\frac{1}{2}\sum_{m,n=1}^{3}w_{mn}P_mP_n\right]F(\mathbf{r})=\varepsilon F(\mathbf{r})\ . \tag{6}$$

For an ellipsoidal valley, the solution is greatly simplified by the boundary condition that $F$ vanish at and beyond the confining heterojunctions.[13,14] Under this condition the following envelope function is obtained for a state in the $j$th subband:[13]

$$F_j(\mathbf{r})=\psi_j(z)\frac{\exp[i(k_xx+k_yy)]}{(L_xL_y)^{1/2}}\exp[-i(k_{xy}z)]\ , \tag{7}$$

where $k_{xy}=(w_{xz}k_x+w_{yz}k_y)/w_{zz}$, and $\psi_j(z)$ specifies the variation of $F$ along the $z$ axis. We have taken the $z$ axis to be perpendicular to the plane of the quantum well, and have normalized the wave function in the plane in a square of dimension $L_xL_y$. The functions $\psi_j(z)$ are the solutions to

$$-\frac{\hbar^2w_{zz}}{2}\frac{d^2\psi_j}{dz^2}=\gamma_j\psi_j\ , \tag{8}$$

where $\gamma_j$ is the $z$ component of the total energy for the $j$th state. The total energy $\varepsilon_j$ is the sum of $\gamma_j$ and a transverse energy $\varepsilon_t$ which is given by the expression[13]

$$\varepsilon_t=\frac{\hbar^2}{2}\left[\left[w_{xx}-\frac{w_{xz}^2}{w_{zz}}\right]k_x^2+2\left[w_{xy}-\frac{w_{xz}w_{yz}}{w_{zz}}\right]k_xk_y+\left[w_{yy}-\frac{w_{yz}^2}{w_{zz}}\right]k_y^2\right]\ . \tag{9}$$

For a quantum well that extends from $z=0$ to $L_z$, the boundary conditions $\psi(z\geq L_z)=0$ and $\psi(z\leq 0)=0$ lead to the wave functions $\psi_j(z)=(2/L_z)^{1/2}\sin(\kappa_jz)$, where $\kappa_j=j\pi/L_z$. This "infinite-barrier approximation" for the wave functions allows the explicit calculation of the intersubband transitions between these states, but is not expected to greatly diminish the accuracy of the calculation. We will apply this approximation consistently, despite the fact that for one of the materials to be analyzed (spherical-valley GaAs), the envelope functions can be calculated exactly for a quantum well having barriers of finite height. This procedure will put all of the calculations on equal footing, thus permitting valid comparisons between different quantum-well materials.

## IV. INTERSUBBAND TRANSITION RATE

Under the influence of the perturbation $H_P(t)$, the term of the harmonic vector potential varying with time as $e^{-i\omega t}$ can cause the transition of an electron in a state $|F_1\rangle$ in the first subband of the quantum well to a state $|F_2\rangle$ in the second subband. For a sufficiently small magnitude of $H_P$, the transition rate from $|F_1\rangle$ to $|F_2\rangle$ is given by Fermi's golden rule of time-dependent perturbation theory,

$$R_{12}=\frac{2\pi}{\hbar}|H_{21}|^2\delta(\varepsilon_2-\varepsilon_1-\hbar\omega)\ , \tag{10}$$

where $H_{21}=\langle F_2|H_P|F_1\rangle$. In the present treatment we assume that the harmonic vector potential acts along with scattering events that are assumed to occur at an average rate $\tau_s^{-1}$ for each electron in the quantum well. In this case, the following generalized form of Eq. (10) is applicable:[15]

$$R_{12}=\frac{2\pi}{\hbar}|H_{21}|^2\frac{\Gamma_s/2\pi}{(\varepsilon_2-\varepsilon_1-\hbar\omega)^2+\Gamma_s^2/4}\ , \tag{11}$$

where $\Gamma_s$ is the energy-broadening parameter, and is related to the scattering rate by $\Gamma_s=\hbar/\tau_s$.

We evaluate the matrix element $H_{21}$ by first making the assumption, $e^{i\boldsymbol{\beta}\cdot\mathbf{r}}=1$, in Eq. (5). This assumption is valid under two conditions: (1) the longitudinal component of photon momentum is much smaller than $\hbar\kappa_1$ (i.e., $\beta_zL_z\ll 1$), and (2) the transverse component of photon momentum induces a change in the electron energy

that is much less than $\hbar\omega$. Both of these conditions are satisfied in typical semiconductor quantum wells.[16] Our next step in the evaluation of $H_{21}$ is to note that each of the terms in Eq. (4) that does not depend on $P_z$ (i.e., $n \neq 3$) leads to a vanishing contribution to the overall matrix element because of the orthogonality of $\psi_2(z)$ and $\psi_1(z)$ over the range $0$–$L_z$. The three terms with $n=3$ yield a nonvanishing contribution of the following form:

$$\langle F_2|H_P|F_1\rangle = \sum_{m=1}^{3} \frac{2e\hbar}{c} \frac{w_{mz} A_m i\kappa_1}{L_x L_y L_z} \int_0^{L_z} \int_{-L_y/2}^{L_x/2} \int_{-L_x/2}^{L_x/2} e^{i(k_{x1}-k_{x2})x} e^{i(k_{y1}-k_{y2})y} e^{i(k_{xy2}-k_{xy1})z} \times \sin(\kappa_2 z)\cos(\kappa_1 z)dx\,dy\,dz \ . \tag{12}$$

If we carry out the integrations over the $x$ and $y$ coordinates and let $L_x$ and $L_y$ be sufficiently large, we obtain the factors $L_x\delta_{k_{x2},k_{x1}}$ and $L_y\delta_{k_{y2},k_{y1}}$, where $\delta$ is the Kronecker delta function. Evaluation of the integral over the $z$ coordinate then yields a transition rate of the form

$$R_{12} = \frac{64\hbar e^2\kappa_1^2}{9\pi^2 c^2} \frac{(A_x w_{xz} + A_y w_{yz} + A_z w_{zz})^2 \Gamma_s}{(\varepsilon_2-\varepsilon_1-\hbar\omega)^2+\Gamma_s^2/4} \times \delta_{k_{x2},k_{x1}}\delta_{k_{y2},k_{y1}} \ . \tag{13}$$

The overall transition rate per unit area, $S_{12}$, is obtained by summing $R_{12}$ over both subbands and weighting by the probability of occupancy in subband 1 and the probability of vacancy in subband 2:

$$S_{12} = \frac{1}{L_x L_y} \sum_{\mathbf{k}_1} \sum_{\mathbf{k}_2} R_{12} f(\varepsilon_1)[1-f(\varepsilon_2)] \ , \tag{14}$$

where $f$ is the Fermi function. For practical purposes, we assume that the second subband is unoccupied [i.e., $f(\varepsilon_2)=0$] and sum over the second-subband transverse $(k_{x2},k_{y2})$ states. The condition of momentum conservation, represented by the Kronecker $\delta$ functions, couples each state in the second subband to only one in the first subband, so that the double sum reduces to a single sum over the first subband. Furthermore, the application of transverse momentum conservation and Eq. (9) leads to $\varepsilon_2-\varepsilon_1=\gamma_2-\gamma_1$, and we obtain

$$S_{12} = \frac{64\hbar e^2\kappa_1^2}{9\pi^2 c^2 L_x L_y} \frac{(A_x w_{xz} + A_y w_{yz} + A_z w_{zz})^2 \Gamma_s}{(\gamma_2-\gamma_1-\hbar\omega)^2+\Gamma_s^2/4} \times \sum_{\mathbf{k}_1} f[\varepsilon_1(\mathbf{k}_1)] \ . \tag{15}$$

We convert this sum to an integral by multiplying by the two-dimensional density of states $2L_xL_y/4\pi^2$ (factor of 2 in numerator for spin degeneracy), and by taking $L_x$ and $L_y$ to infinity. These steps result in

$$S_{12} = \frac{64\hbar e^2\kappa_1^2}{9\pi^2 c^2} \frac{(A_x w_{xz} + A_y w_{yz} + A_z w_{zz})^2 \Gamma_s}{(\gamma_2-\gamma_1-\hbar\omega)^2+\Gamma_s^2/4} \times \left[\frac{1}{2\pi^2}\int_0^{\infty} f(\varepsilon_1(\mathbf{k}_1))d\mathbf{k}_1\right] \ . \tag{16}$$

The quantity in large parentheses is the sheet density $\sigma$, and evaluates to[14]

$$\sigma = \frac{k_B T}{\pi\hbar^2} m_d \ln\{1+\exp[(\varepsilon_F-\gamma_1)/kT]\} \ , \tag{17}$$

where $\varepsilon_F$ is the Fermi energy, and $m_d$ is the density-of-states mass in the transverse plane of the quantum well for the conduction-band valley which the electron occupies.

We expect that the infinite-barrier approximation leads to an underestimation of the transition rate compared to the rate for real, finite barriers. This is because the envelope functions extend far into finite barriers, such that the transition matrix element $H_{21}$ is larger than predicted by Eq. (12) for the same well width. This matrix element cannot be calculated for ellipsoidal-valley quantum wells with finite barriers because the exact forms of the envelope functions are not known. In quantum wells made of spherical-valley materials (e.g., GaAs) for which exact envelope wave functions are known, finite-barrier and infinite-barrier calculations can be compared directly.[17] In this case, a calculation for finite barriers yields a larger transition-matrix element, or similarly, a larger dipole moment than a calculation for infinite barriers, as expected.

## V. ABSORPTION STRENGTH

### A. Fractional absorption

An experimentally measurable quantity is the fractional absorption per quantum well, $\zeta$, as a function of frequency $\omega$. This is found by summing over ellipsoids and normalizing to the incident photon flux

$$\zeta(\omega) = \frac{\hbar\omega}{I} \sum_{\eta=1}^{M_C} S_{12}^{(\eta)} \ , \tag{18}$$

where $\eta$ is the ellipsoid index, and $M_C$ is the number of ellipsoids that contribute to the absorption at frequency $\omega$. The intensity $I$ is related to the harmonic plane-wave form of the vector potential by $I = n|\mathbf{A}|^2\omega^2/(2\pi c)$, where $n$ is the refractive index of the quantum-well material. This leads to the expression

$$\zeta(\omega) = \frac{128\hbar^2 e^2}{9\pi n\omega c} \times \sum_{\eta=1}^{M_C} \frac{(A_x w_{xz}^{(\eta)} + A_y w_{yz}^{(\eta)} + A_z w_{zz}^{(\eta)})^2}{|\mathbf{A}|^2} \times \frac{\kappa_{1\eta}^2 \sigma_\eta \Gamma_{s\eta}}{(\gamma_{2\eta}-\gamma_{1\eta}-\hbar\omega)^2+\Gamma_{s\eta}^2/4} \ . \tag{19}$$

In general, each ellipsoid has a first-state energy $\gamma_1^{(\eta)}$ that depends on the spatial orientation of the ellipsoid through the term $w_{zz}^{(\eta)}$. In the present treatment, we will evaluate Eq. (19) for the special case that only the ellipsoid with the lowest $\gamma_1^{(\eta)}$ is occupied. For certain symmetric crystal orientations, several or all of the ellipsoids may share the same value of minimum $\gamma_1$. In any case, $M_C$ becomes the degeneracy of the first state, i.e., the number of ellipsoids that have the minimum $\gamma_1$. Each of these ellipsoids necessarily has the same value of $w_{zz}$ and $\gamma_2-\gamma_1$ because the infinite-barrier approximation makes $\kappa_1$ and $\kappa_2$ independent of ellipsoid orientation. Thus we can write $\kappa_1^2=2(\gamma_2-\gamma_1)/3\hbar^2 w_{zz}=2\omega_0/3\hbar w_{zz}$, where $\omega_0$ is the intersubband Bohr frequency. Furthermore, symmetry considerations dictate that all ellipsoids with the same principal masses ($m_l$ and $m_t$) and oriented to have the same $w_{zz}$ component, must also share a common value of transverse density-of-states mass $m_d$.[13] The electron population is then equally distributed among the first-state ellipsoids. These facts lead to the following expression:

$$\zeta(\omega)=\frac{256\hbar e^2\omega_0\sigma_T}{27\pi nc\omega M_C w_{zz}}\frac{\Gamma_s}{(\hbar\omega_0-\hbar\omega)^2+\Gamma_s^2/4}\times\sum_{\eta=1}^{M_C}\frac{(A_x w_{xz}^{(\eta)}+A_y w_{yz}^{(\eta)}+A_z w_{zz}^{(\eta)})^2}{|\mathbf{A}|^2}, \quad (20)$$

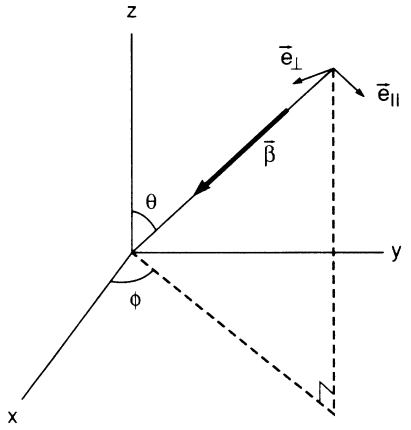


FIG. 1. Spherical coordinate system for analyzing the dependence of absorption on the polarization of an incident plane wave characterized by $\boldsymbol{\beta}$. $\mathbf{e}_\perp$ and $\mathbf{e}_{||}$ are the unit vectors into which any linearly polarized vector potential $\mathbf{A}$ (lying normal to $\boldsymbol{\beta}$) can be decomposed. The $x$ and $y$ axes are oriented with respect to the conventional cubic unit cell of the quantum-well material, as described in the Appendix.

where $\sigma_T=\sum_{\eta=1}^{M_C}\sigma_\eta$ is the total sheet charge density in the first state. For $\Gamma_s \ll \hbar\omega_0$, the maximum value of this expression occurs very near $\omega=\omega_0$, and is well approximated by

$$\zeta(\omega_0)=\frac{1024\hbar e^2\sigma_T}{27\pi nc\Gamma_s M_C w_{zz}}\sum_{\eta=1}^{M_C}\frac{(A_x w_{xz}^{(\eta)}+A_y w_{yz}^{(\eta)}+A_z w_{zz}^{(\eta)})^2}{|\mathbf{A}|^2}=\frac{\hbar\sigma_T}{\Gamma_s}\left[\frac{1024e^2 w_{zz}G(\theta,\phi)}{27\pi nc}\right]. \quad (21)$$

The function $G(\theta,\phi)$, which we call the crystallographic factor, is given by the dimensionless expression

$$G(\theta,\phi)=\frac{w_{zz}^{-2}}{M_C}\sum_{\eta=1}^{M_C}\frac{(A_x w_{xz}^{(\eta)}+A_y w_{yz}^{(\eta)}+A_z w_{zz}^{(\eta)})^2}{|\mathbf{A}|^2}. \quad (22)$$

It does not depend on impurity concentration, temperature, or intrinsic scattering processes, so that it is useful in analyzing the different crystal structures and quantum-well orientations considered in this paper. The quantity in Eq. (21) in large parentheses is useful for comparing specific quantum-well materials.

Because of the two-dimensional nature of the quantum well, the fractional absorption may be a strong function of both the propagation direction and the polarization of the incident radiation. We characterize the polarization in the conventional way shown in Fig. 1. A linearly polarized $\mathbf{A}$, normal to $\boldsymbol{\beta}$, is resolved into two components $A_{||}$ and $A_\perp$ that are parallel and perpendicular, respectively, to the plane of incidence, which is defined by $\boldsymbol{\beta}$ and the $z$ axis. The spherical coordinate system shown in Fig. 1 leads to the relations $A_x=\cos\theta\cos\phi\, A_{||}+\sin\phi\, A_\perp$, $A_y=\cos\theta\sin\phi\, A_{||}-\cos\phi\, A_\perp$, and $A_z=-\sin\theta\, A_{||}$. The orientation of the $x$ and $y$ axes in the plane of the quantum well is chosen to take advantage of any symmetry in the effective-mass tensor for the quantum-well material.

### B. Absorption coefficient

The fractional absorption given by Eq. (21) is valid for any orientation of the plane wave relative to the quantum well, but it does not reflect the length over which the fraction absorption occurs. This length is highly dependent on the direction of propagation $\boldsymbol{\beta}$ because of the small extent of the quantum well along the $z$ axis. For example, suppose a quantum well of width $L_z$ yields the same fractional absorption for radiation incident normal to the plane of the quantum well and at an angle $\theta$ with respect to the normal. From geometrical considerations alone, the absorption will occur over a length $L_z$ in the former case, and over a length $L_z\sec\theta$ in the latter case.

We call $L_z\sec\theta$ the length of absorption, and use it to define a directionally dependent absorption coefficient (Fig. 2):

$$\exp[-\alpha(\omega)L_z\sec\theta]=1-\zeta(\omega). \quad (23)$$

We have assumed implicitly that the magnitude of the vector potential decays negligibly across the width of the quantum well (i.e., between $z=0$ and $z=L_z$). This is equivalent to $\zeta(\omega)\ll 1$, which leads to the approximate

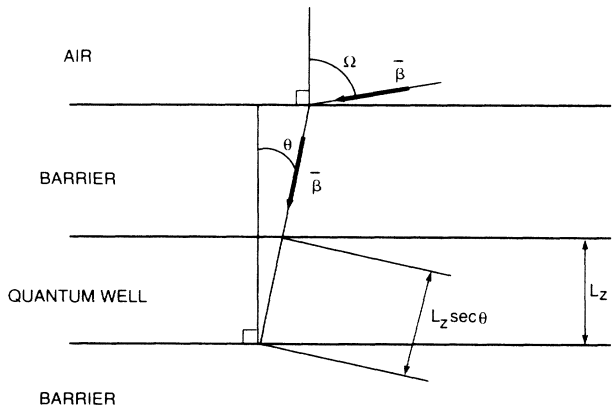


FIG. 2. Cross-sectional view of quantum well of width $L_z$. $L_z\sec\theta$ is the length of absorption.

expression for the absorption coefficient, $\alpha(\omega)=\zeta(\omega)/L_z\sec\theta$. From the infinite-barrier approximation, $L_z=(3\hbar\pi^2 w_{zz}/2\omega_0)^{1/2}$. These relations and Eq. (21) lead to the following expression for the absorption coefficient at $\omega=\omega_0$:

$$\alpha(\omega_0)=\frac{\hbar\sigma_T}{\Gamma_s}\left[\frac{1024\xi(2\hbar\omega_0 w_{zz}/3)^{1/2}}{27\pi^2 n}\cos\theta\, G(\theta,\phi)\right], \tag{24}$$

where $\xi=e^2/\hbar c\cong\frac{1}{137}$ is the fine-structure constant. Note that the absorption coefficient decreases to zero as $\theta$ approaches 90°. This can be understood from further geometrical considerations. Our derivation has been carried out for an ideal plane wave that, by definition, has infinite lateral extent. However, the quantum well necessarily has a finite width. Therefore, as $\theta$ approaches 90°, the quantum well intercepts an infinitesimal fraction of the plane wave or, equivalently, the geometrical filling factor of the quantum well approaches zero. This appears to be inconsistent with the result, derived later, that the crystallographic factor for the $A_\parallel$ component has its largest value at $\theta=90°$ for many of the quantum-well configurations analyzed. We resolve the apparent inconsistency by noting that a real beam of light impinging on the quantum well at $\theta=90°$ is, in the sense of Fourier optics, a distribution of plane waves of different spatial frequencies. Each spatial frequency (except the dc component) corresponds to a plane wave incident at a $\theta$ different than 90°, so that the absorption of the beam as a whole is nonzero.

### C. Crystal structure and quantum-well orientation

Although Eq. (21) can be applied to any material in which the electrons occupy ellipsoidal valleys, we will deal only with a subset of this class characterized by cubic crystal symmetry. The following three band structures are analyzed: (1) conduction-band minimum located at $k=0$ with a spherical constant-energy surface ($\Gamma$-valley material), (2) conduction-band minima located along the equivalent $\langle 100\rangle$ axes near the $X$ points ($X$-valley material), and (3) conduction-band minima located along the equivalent $\langle 111\rangle$ axes at the $L$ points ($L$-valley material). For $X$-valley materials there are six separate ellipsoids, while for $L$-valley materials there are four separate ellipsoids consisting of a half ellipsoid located at each of eight equivalent $L$ points.

We will evaluate Eq. (21) for quantum wells grown on each of three low-index planes: (100), (111), and (011). For each of the assumed material types, the crystallographic factor for the two polarization components can be obtained by deriving the elements of the reciprocal effective-mass tensor in a coordinate system defined by the conventional cubic unit cell. This derivation is car-

TABLE I. Crystallographic factor $G(\theta,\phi)$ defined by Eq. (22) and derived in the Appendix. $\mathbf{A}_\parallel$ and $\mathbf{A}_\perp$ are the components of the vector potential that are parallel and perpendicular, respectively, to the plane of incidence defined by $\boldsymbol{\beta}$ and the $z$ axis in Fig. 1. $m_{lt}=(m_l m_t)/(m_l-m_t)$.

| Material | Polarization | Quantum-well orientation (100) | (111) | (011) |
|---|---|---|---|---|
| $\Gamma$-valley | $\mathbf{A}_\perp$ | 0 | 0 | 0 |
| | $\mathbf{A}_\parallel$ | $\sin^2\theta$ | $\sin^2\theta$ | $\sin^2\theta$ |
| $X$-valley | $\mathbf{A}_\perp$ | 0 | $\dfrac{w_{zz}^{-2}}{9m_{lt}^2}$ | $\dfrac{w_{zz}^{-2}\cos^2\phi}{4m_{lt}^2}$ |
| | $\mathbf{A}_\parallel$ | $\sin^2\theta$ | $\dfrac{w_{zz}^{-2}\cos^2\theta}{9m_{lt}^2}+\sin^2\theta$ | $\dfrac{w_{zz}^{-2}\cos^2\theta\sin^2\phi}{4m_{lt}^2}+\sin^2\theta$ |
| $L$-valley | $\mathbf{A}_\perp$ | $\dfrac{w_{zz}^{-2}}{9m_{lt}^2}$ | 0 | $\dfrac{2w_{zz}^{-2}\sin^2\phi}{9m_{lt}^2}$ |
| | $\mathbf{A}_\parallel$ | $\dfrac{w_{zz}^{-2}\cos^2\theta}{9m_{lt}^2}+\sin^2\theta$ | $\sin^2\theta$ | $\dfrac{2w_{zz}^{-2}\cos^2\theta\cos^2\phi}{9m_{lt}^2}+\sin^2\theta$ |

ried out in the Appendix, and the resulting factors are compiled in Table I. Some of these results deserve emphasis. The crystallographic factors for a Γ-valley material in all three quantum-well orientations imply zero absorption of light at normal incidence to the quantum-well plane. An $X$-valley material in a (100) quantum well and an $L$-valley material in a (111) quantum well display the same behavior. This follows from the fact that the off-diagonal components $w_{xz}$ and $w_{yz}$ vanish for each ellipsoid. In contrast, both an $X$-valley material in a (111) well and an $L$-valley material in a (100) well can absorb normally incident light. There exists no azimuthal dependence of this absorption because the $z$ axis is a threefold rotation axis in the $X$-valley (111) well and a fourfold axis in the $L$-valley (100) well. However, azimuthal dependence is predicted for both $X$- and $L$-valley materials in (011) quantum wells because the $z$ axis is then a twofold rotation axis.

## VI. EXAMPLES

### A. GaAs

To establish the validity of the present formalism, we first calculate the fractional absorption and absorption coefficient for Γ-valley GaAs quantum wells, since there are sufficient experimental data for (100) GaAs wells to permit a significant comparison with theory. Our calculation is carried out for the technologically important wavelength of $\lambda=10\ \mu$m. The GaAs quantum-well width that yields a maximum first-to-second-state absorption at this wavelength is $L_z=11.6$ nm, according to the infinite-barrier approximation. Most of the electrons in a moderately doped GaAs quantum well of this width occupy the first state. If we substitute the appropriate Γ-valley crystallographic factors from Table I into Eq. (21) along with the values $w_{zz}^{-1}=0.067m_0$ and $n=\sqrt{10.9}$, we obtain $\zeta(\omega_0)=0.46(\hbar\sigma_T/\Gamma_s)\sin^2\theta$ and $\alpha(\omega_0)=3.9\times10^5(\hbar\sigma_T/\Gamma_s)\cos\theta\sin^2\theta\ \mathrm{cm}^{-1}$ for the $A_\parallel$ component, and $\zeta=\alpha=0$ for the $A_\perp$ component. The maximum absorption coefficient with respect to $\theta$ is $\alpha=1.5\times10^5(\hbar\sigma_T/\Gamma_s)\ \mathrm{cm}^{-1}$ at $\theta=\sin^{-1}\sqrt{2/3}=54.7°$.

We compare our prediction with the experimental results for a (100) GaAs quantum well obtained by Levine *et al.*,[18] who measured $\alpha$ at a wavelength of $\lambda\cong10\ \mu$m for light incident at 45°, polarized in the plane of incidence. Substituting the values of $\sigma_T=7.6\times10^{11}\ \mathrm{cm}^{-2}$ and $\Gamma_s=11$ meV given by Levine *et al.*, we predict $\zeta(\omega_0)=0.010$ and $\alpha(\omega_0)=6.4\times10^3\ \mathrm{cm}^{-1}$ for the given illumination conditions. The latter value is in good agreement with their experimental value of $7.1\times10^3\ \mathrm{cm}^{-1}$.[19]

### B. Si and Ge

Silicon is an $X$-valley material for which the six constant-energy ellipsoids are characterized by a principal transverse mass $m_t=0.19m_0$ and a principal longitudinal mass $m_l=0.98m_0$.[20] These mass values are entered in Table II along with the other fundamental material parameters required to calculate the absorption strength. Table III gives the calculated peak fractional absorption and corresponding well width for 10-$\mu$m radiation incident on (100), (111), and (011) quantum wells. In each case the well width is that value found by using the appropriate $w_{zz}$ values in Table II and the infinite-barrier approximation. For the (111) orientation, the peak fractional absorption of normally incident light is $\zeta(\omega_0)=0.015\hbar\sigma_T/\Gamma_s$ per quantum well, independent of azimuthal angle. For the (011) orientation, we find $\zeta(\omega_0)=0.042\hbar\sigma_T/\Gamma_s$ with the incident field oriented along $[01\bar{1}]$, and $\zeta(\omega_0)=0$ with the field along [100].

Germanium is an $L$-valley material with four constant-energy ellipsoids having the principal mass values $m_t=0.082m_0$ and $m_l=1.64m_0$.[20] The (100) and (011) quantum-well orientations yield absorption at normal incidence. The $\lambda=10\ \mu$m fractional absorptions and well widths for these orientations are given in Table III. From Table I, we see that the geometrical characteristics of the absorption are very similar to those for (111) and (011) Si quantum wells. However, in both cases the absorption strength for Ge is at least three times that for Si. This difference is caused primarily by the greater eccentricity of the Ge ellipsoids.

### C. AlGaAs

The $Al_xGa_{1-x}As$ alloys with $x\gtrsim0.45$ are $X$-valley materials.[21] We consider an alloy with a large enough Al fraction that the first Γ state has a much higher energy than the first $X$ state, and thus contains a negligible fraction of the total sheet charge. Mixing between this Γ

TABLE II. Fundamental quantities for selected quantum-well materials. $w_{zz}$ is a reciprocal effective-mass tensor component for the ground state of each quantum well in the infinite-barrier approximation.

| Quantity | Si ($X$) | Ge ($L$) | $Al_{0.5}Ga_{0.5}As$ ($X$) | $Al_{0.3}Ga_{0.7}Sb$ ($L$) |
|---|---|---|---|---|
| $n$ | 3.45[a] | 4.0[a] | 3.30[b] | 3.80[b] |
| $m_l$ | 0.98[a] | 1.64[a] | 1.20[c] | 1.20[d] |
| $m_t$ | 0.19[a] | 0.082[a] | 0.21[c] | 0.08[d] |
| $m_{lt}$ | 0.236 | 0.086 | 0.25 | 0.086 |
| $w_{zz}^{-1}$ (100) | 0.98 | 0.12 | 1.20 | 0.12 |
| $w_{zz}^{-1}$ (111) | 0.26 | 1.64 | 0.29 | 1.20 |
| $w_{zz}^{-1}$ (011) | 0.32 | 0.22 | 0.36 | 0.21 |

[a]Reference 20.
[b]Reference 26.
[c]Reference 22.
[d]Reference 23.

TABLE III. Peak fractional absorption and width of selected quantum wells for $\lambda = 10$-$\mu$m radiation at normal incidence.

| Orientation | Quantity | Si ($X$) | Ge ($L$) | $Al_{0.5}Ga_{0.5}As$ ($X$) | $Al_{0.3}Ga_{0.7}Sb$ ($L$) |
|---|---|---|---|---|---|
| (100) | $\zeta(\omega_0)\times\Gamma_s/\hbar\sigma_T$ | 0 | 0.046 | 0 | 0.048 |
| | $L_z$ (nm) | 3.0 | 8.7 | 2.8 | 8.7 |
| (111) | $\zeta(\omega_0)\times\Gamma_s/\hbar\sigma_T$ | 0.015 | 0 | 0.016 | 0 |
| | $L_z$ (nm) | 5.9 | 2.4 | 5.6 | 2.8 |
| (011) | $\zeta(\omega_0)\times\Gamma_s/\hbar\sigma_T$ | $0.042\sin^2\phi$ | $0.168\cos^2\phi$ | $0.044\sin^2\phi$ | $0.169\cos^2\phi$ |
| | $L_z$ (nm) | 5.3 | 6.4 | 5.0 | 6.6 |

state and the first or second $X$ state is ignored in the present treatment. We choose an alloy with $x = 0.5$, for which the exact values of the principal masses of the ellipsoids are not known. Thus we estimate them by linear interpolation between the GaAs and AlAs values.[22] This procedure yields $m_t = 0.21m_0$ and $m_l = 1.2m_0$.

The (111) AlGaAs quantum well, like (111) Si, absorbs light incident normal to the plane. The fractional absorption of (111) AlGaAs for $\lambda = 10$ $\mu$m and $L_z = 5.6$ nm (Table III) is $\zeta(\omega_0) = 0.016\hbar\sigma_T/\Gamma_s$ per quantum well, so that the absorption per electron is nearly identical to that of (111) Si. For $\sigma_T = 7.6\times10^{11}$ cm$^{-2}$ and $\Gamma_s = 11$ meV, the fractional absorption is 0.000 73, about 13 times lower than the value for a (100) GaAs quantum well at 45° incidence. However, the (111) AlGaAs exhibits this absorption for all polarizations and at normal incidence, whereas the GaAs well absorbs just the $A_\parallel$ component and only at oblique incidence.

### D. AlGaSb

While there is no AlGaAs alloy that is an $L$-valley material, $Al_xGa_{1-x}Sb$ is an $L$-valley material for $0.25 \lesssim x \lesssim 0.55$. Because the values of the principal $L$-valley masses are not known for the AlGaSb alloys, we assume that these masses are equal to the values obtained by a $\mathbf{k}\cdot\mathbf{p}$ calculation for GaSb:[23] $m_t = 0.08m_0$ and $m_l = 1.2m_0$. As in the treatment of the AlGaAs well, the Al fraction is assumed to be large enough so that the first $\Gamma$ state is unoccupied, and any mixing between this $\Gamma$ state and either $L$ state is ignored.

The most practical AlGaSb quantum-well orientation is the (100) since this is the one most commonly used for the AlGaSb crystal growth. Use of the appropriate crystallographic factors, as listed in Table I, yields a fractional absorption of $\zeta(\omega_0) = 0.048\hbar\sigma_T/\Gamma_s$ for normally incident $\lambda = 10$-$\mu$m light and for $L_z = 8.7$ nm. This absorption is three times larger per electron than in the (111) AlGaAs well. For the same values of $\sigma_T$ and $\Gamma_s$ as used for the AlGaAs well, we calculate $\zeta(\omega_0) = 0.022$ for any polarization of light at normal incidence.

The (011) AlGaSb quantum well is not as practical as the (100) well, but it yields higher absorption. From Table III, we see that the peak fractional absorption of normally incident light at $\lambda = 10$ $\mu$m is given by $0.169(\hbar\sigma_T/\Gamma_s)\cos^2\phi$. At $\phi = 0$ this is about four times larger than the fractional absorption of the (011) AlGaAs quantum well at $\phi = \pi/2$, and is also about four times larger than the azimuthally independent absorption of the (100) AlGaSb well. Thus the (011) AlGaSb quantum well could be very useful in applications that utilize linearly polarized light at normal incidence.

The enhancement of absorption for AlGaSb compared to AlGaAs is caused primarily by the greater eccentricity of the $L$-valley ellipsoids compared to the $X$-valley ellipsoids—the same reason that (100) Ge exhibits greater absorption than (111) Si. Physically, the greater eccentricity of the $L$ ellipsoids leads to a greater coupling between a force applied along a nonprincipal direction and a momentum change in the plane perpendicular to the force.

## VII. DISCUSSION

By providing the capability for absorbing light at normal incidence, the ellipsoidal-valley materials can overcome the difficulties encountered in coupling radiation to quantum wells in $\Gamma$-valley materials such as GaAs. According to our theory, the absorption coefficient of $\Gamma$-valley wells is proportional to $\cos\theta\sin^2\theta$, so that the maximum absorption coefficient $\alpha_{\max}$ occurs for $\theta = 54.7°$. If we assume that the light passes through a semiconductor-air interface with an angle of incidence $\Omega$ before impinging on the quantum well (Fig. 2), then Snell's law of refraction limits the maximum $\theta$ to the value $\sin^{-1}(n^{-1})$ for $\Omega = 90°$. If $n$ is large, as in most semiconductors, this angle is much less than 54.7°. Therefore the highest absorption coefficient that can be obtained is $\alpha_{\max}$ divided by the factor $2n^2/\{3\sqrt{3}\cos[\sin^{-1}(n^{-1})]\}$. For GaAs with $n = 3.3$, this factor is 4.4. In practice, $\Omega$ is chosen to be no larger than Brewster's angle, $\Omega_B = \tan^{-1}n$, to avoid a prohibitively high reflection coefficient. For $\Omega = \Omega_B$, the absorption coefficient for GaAs is 4.8 times less than $\alpha_{\max}$. One way to avoid this reduction is to modify the topography of the wafer surface. For example, an angled facet can be lapped into the edge of the wafer—the procedure followed in making the GaAs quantum-well measurements

at $\theta=45°$.[18] It is also possible to etch two-dimensional triangular gratings into the wafer surface by using selective wet etchants.[24] However, both of these schemes complicate device fabrication and preclude the use of absorption-enhancement techniques such as the application of antireflection coatings to the front surface of the wafer and high-reflection coatings to the back surface.

In addition to Si, Ge, AlGaAs, and AlGaSb, other ellipsoidal-valley materials are potential quantum-well absorbers. For example, GaP is an $X$-valley material with principal mass values comparable to those of Si and AlGaAs. Thus, according to our theory, it could achieve an absorption per electron comparable to that of the latter materials. However, it is doubtful that high-quality GaP quantum wells can be grown at present, since the techniques for epitaxial growth of heterojunctions involving this material are less developed than those for AlGaAs and AlGaSb. Another possibility is the $L$-valley material PbSnTe, a rocksalt-structure IV-VI alloy, which has much smaller principal masses [$m_l \cong 0.22m_0$ and $m_t \cong 0.028m_0$ for $n$-PbTe with a carrier concentration of $3.0\times10^{18}$ cm$^{-3}$ (Ref. 25)] than the other materials considered. For (100) quantum wells, these masses yield $m_{lt}=0.034m_0$ and $w_{zz}^{-1}=0.042m_0$, which lead to an absorption coefficient per electron about 30% greater than that of AlGaSb.

Finally, we note that the III-V materials discussed here have an important advantage over Si and Ge, since the III-V quantum wells can be lattice matched to the barrier material and to the substrate. In the case of AlGaAs, lattice matching is automatic, since GaAs and AlAs have nearly equal lattice constants. For AlGaSb, lattice matching to GaSb can be achieved by incorporating a small fraction of As to make the quaternary alloy $Al_xGa_{1-x}As_ySb_{1-y}$. For example, $Al_{0.55}Ga_{0.45}Sb$ has a 0.36% mismatch relative to GaSb, but $Al_{0.55}Ga_{0.45}As_{0.05}Sb_{0.95}$ is lattice matched to GaSb. Such a small change in composition has an insignificant effect on the band structure, but should eliminate strain-induced defects (e.g., misfit dislocations).

## VIII. SUMMARY

We have derived general expressions for the fractional absorption and absorption coefficient due to intersubband transitions by electrons confined to a quantum well. Our formulation applies to any material in which unconfined electrons occupy valleys with ellipsoidal constant-energy surfaces. In the special case of spherical-valley materials such as GaAs, quantum wells absorb only the polarization component that is perpendicular to the plane of the well. In contrast, our theory predicts that ellipsoidal-valley quantum wells can absorb light having any direction of polarization relative to the plane of the well, including light polarized in the plane. The only requirement for this effect is that at least one of the ellipsoids must be oriented in $k$ space such that its principal axes are not collinear with the longitudinal ($k_z$) axis of the well. The physical basis for the effect is that the crystal potential for an electron in an ellipsoidal valley is anisotropic, and thus can couple orthogonal components of the momentum and the vector potential. The strength of

TABLE IV. Reciprocal effective-mass tensor components for $X$-valley materials in quantum wells. $m_{lt}=(m_lm_t)/(m_l-m_t)$.

| Number of ellipsoids | $w_{xz}$ | $w_{yz}$ | $w_{zz}$ |
|---|---|---|---|
| | A. (100) Quantum well | | |
| 2 | 0 | 0 | $\frac{1}{m_l}$ |
| 4 | 0 | 0 | $\frac{1}{m_t}$ |
| | B. (111) Quantum well | | |
| 2 | 0 | $\frac{\sqrt{2}}{3m_{lt}}$ | $\frac{2m_l+m_t}{3m_lm_t}$ |
| 2 | $\frac{1}{\sqrt{6}m_{lt}}$ | $\frac{-1}{3\sqrt{2}m_{lt}}$ | $\frac{2m_l+m_t}{3m_lm_t}$ |
| 2 | $\frac{-1}{\sqrt{6}m_{lt}}$ | $\frac{-1}{3\sqrt{2}m_{lt}}$ | $\frac{2m_l+m_t}{3m_lm_t}$ |
| | C. (011) Quantum well | | |
| 2 | 0 | 0 | $\frac{1}{m_t}$ |
| 2 | 0 | $\frac{-1}{2m_{lt}}$ | $\frac{m_l+m_t}{2m_lm_t}$ |
| 2 | 0 | $\frac{1}{2m_{lt}}$ | $\frac{m_l+m_t}{2m_lm_t}$ |

TABLE V. Reciprocal effective-mass tensor components for $L$-valley materials in quantum wells.

| Number of ellipsoids | $w_{xz}$ | $w_{yz}$ | $w_{zz}$ |
|---|---|---|---|
| | A. (100) Quantum well | | |
| 1 | $\frac{1}{3m_{lt}}$ | $\frac{1}{3m_{lt}}$ | $\frac{2m_l+m_t}{3m_lm_t}$ |
| 1 | $\frac{1}{3m_{lt}}$ | $\frac{-1}{3m_{lt}}$ | $\frac{2m_l+m_t}{3m_lm_t}$ |
| 1 | $\frac{-1}{3m_{lt}}$ | $\frac{1}{3m_{lt}}$ | $\frac{2m_l+m_t}{3m_lm_t}$ |
| 1 | $\frac{-1}{3m_{lt}}$ | $\frac{-1}{3m_{lt}}$ | $\frac{2m_l+m_t}{3m_lm_t}$ |
| | B. (111) Quantum well | | |
| 1 | 0 | 0 | $\frac{1}{m_l}$ |
| 1 | $\frac{-\sqrt{8}}{9m_{lt}}$ | 0 | $\frac{8m_l+m_t}{9m_lm_t}$ |
| 1 | $\frac{\sqrt{2}}{9m_{lt}}$ | $\frac{-\sqrt{2/3}}{3m_{lt}}$ | $\frac{8m_l+m_t}{9m_lm_t}$ |
| 1 | $\frac{\sqrt{2}}{9m_{lt}}$ | $\frac{\sqrt{2/3}}{3m_{lt}}$ | $\frac{8m_l+m_t}{9m_lm_t}$ |
| | C. (011) Quantum well | | |
| 1 | $\frac{-\sqrt{2}}{3m_{lt}}$ | 0 | $\frac{2m_t+m_l}{3m_tm_l}$ |
| 1 | $\frac{\sqrt{2}}{3m_{lt}}$ | 0 | $\frac{2m_t+m_l}{3m_tm_l}$ |
| 2 | 0 | 0 | $\frac{1}{m_t}$ |

this coupling (as expressed by the off-diagonal components of the reciprocal effective-mass tensor) increases with the eccentricity of the ellipsoids, so that $L$-valley materials in (100) quantum wells display greater absorption than $X$-valley materials in (111) wells. At present, the most promising $L$-valley material system appears to be $Al_xGa_{1-x}Sb$ with $0.25 \lesssim x \lesssim 0.55$.

## ACKNOWLEDGMENTS

The authors would like to thank Professor A. L. McWhorter, who offered several important corrections and clarifications of the theoretical derivation, and A. J. Strauss, who provided a very useful critique of the text. The authors also thank D. L. Spears, H. J. Zeiger, and J. P. Mattia for significant contributions, R. A. Murphy, and E. Stern for providing support, and Professor B. Lax and J. W. Bales for helpful discussions. This work was sponsored by the Department of the Air Force, U. S. Department of Defense.

## APPENDIX: DERIVATION OF CRYSTALLOGRAPHIC FACTORS

The crystallographic factors compiled in Table I are obtained by evaluating Eq. (21) in the coordinate system of the conventional cubic unit cell for each of the three material types considered. This requires a derivation of the reciprocal effective-mass tensor components, of which $w_{zz}$ is useful in calculating eigenstate energies, and $w_{xz}$ and $w_{yz}$ are useful in understanding the momentum vector-potential cross coupling.

Because of spherical symmetry, a $\Gamma$-valley material has the tensor components $w_{xz}=0$ and $w_{yz}=0$ for all quantum-well orientations. The reciprocal effective-mass tensor has three identical diagonal components equal to $1/m^*$. Similarly, an $X$-valley material in a (100) quantum well has vanishing $w_{xz}$ and $w_{yz}$ components because the $z$ axis is a principal axis of each ellipsoid. The four ellipsoids lying in the plane have a longitudinal component $w_{zz}=1/m_t$, and the two perpendicular to the plane have $w_{zz}=1/m_l$. These components are given in Table IV. Since $m_l \gg m_t$, electrons in the four ellipsoids in the plane will have (by the infinite-barrier approximation) a lower first-state energy than electrons in the ellipsoids perpendicular to the plane. Summation over the first-state ellipsoids according to Eq. (22) leads to the crystallographic factors given in Table I.

The reciprocal effective-mass tensor for an $X$-valley material in a (111) quantum well is obtained by a similarity transformation. If we choose $\mathbf{e}_x$ and $\mathbf{e}_y$ to lie along the $[1\bar{1}0]$ and $[11\bar{2}]$ axes, respectively, of the conventional cubic unit cell, we obtain the components given in Table IV. As expected from geometrical considerations, the longitudinal component $w_{zz}$ is the same for all ellipsoids, and thus the first state of the quantum well is sixfold degenerate. The crystallographic factors for this first state are given in Table I.

An $X$-valley material in a (011) quantum well has a four-fold-degenerate first state. By choosing $\mathbf{e}_x$ and $\mathbf{e}_y$ to lie along the [100] and $[01\bar{1}]$ axes, respectively, of the unit cell, the four ellipsoids that contribute electrons to this state are found to have the tensor components given in Table IV. From the crystallographic factors given in Table I, it is clear that the absorption is zero for light polarized along the [100] axis, and is a maximum for light polarized along $[01\bar{1}]$ or $[0\bar{1}1]$.

The tensor components for an $L$-valley material in a (100) quantum well are easily determined by choosing $\mathbf{e}_x$ along [100] and $\mathbf{e}_y$ along [010]. As shown in Table V, the longitudinal components are all identical, so that the first state of the well is fourfold degenerate. The crystallographic factors for this state are identical to those for the $X$-valley (111) quantum well.

An $L$-valley material in a (111) quantum well is somewhat more complicated than the above configurations, but the results are very similar. The $x$ and $y$ axes of the quantum-well coordinate system are chosen to lie along $[11\bar{2}]$ and $[\bar{1}10]$, respectively. The ellipsoid lying normal to the plane has vanishing off-diagonal tensor components and $w_{zz}=1/m_l$. Electrons in this ellipsoid will occupy the first state of the quantum well. The other three ellipsoids have identical longitudinal components in agreement with Stern and Howard,[13] and nonzero off-diagonal components given in Table V. These ellipsoids thus define a threefold-degenerate state that may or may not be the second level in the well, depending on the well width (the second and possibly some higher levels of the longitudinal ellipsoid could lie lower). The crystallographic factors for this state are consistent with absorption at normal incidence, and are given by $4w_{zz}^{-2}/81m_{lt}^2$ and $4w_{zz}^{-2}\cos^2\theta/81m_{lt}^2+\sin^2\theta$ for the $A_\perp$ and $A_\parallel$ components, respectively. The weakness of these factors, in comparison to those for (100) wells of $L$-valley materials and (111) wells of $X$-valley materials, follows from the fact that the three-fold degenerate ellipsoids lie very nearly in the plane of the well. Thus they have small $w_{xz}$ and $w_{yz}$ components, as shown in Table V. The crystallographic factors do retain the azimuthal independence of the other structures, because in this case the [100] axis is a threefold rotation axis.

The final structure we analyze is an $L$-valley material in a (011) quantum well. The crystallographic factors are similar to those for the $X$-valley (011) quantum well, except that now only two ellipsoids contribute to the first state. If we again choose $\mathbf{e}_x$ and $\mathbf{e}_y$ to lie along the [100] and $[01\bar{1}]$ directions, respectively, we find the $w_{ij}$ components for these ellipsoids given in Table V, and the crystallographic factors listed in Table I.

[1]L. C. West and S. J. Eglash, Appl. Phys. Lett. **46**, 1156 (1985).
[2]B. F. Levine, C. G. Bethea, G. Hasnain, J. Walker, and R. J. Malik, Appl. Phys. Lett. **53**, 296 (1988).
[3]M. Helm, E. Colas, P. England, F. DeRosa, and S. J. Allen, Jr., Appl. Phys. Lett. **53**, 1714 (1988).
[4]T. Ando, T. Eda, and M. Nakayama, Solid State Commun. **23**, 751 (1977).
[5]A. Kamgar, Solid State Commun. **21**, 823 (1977).

[6]T. Cole and B. D. McCombe, Phys. Rev. B **29**, 3180 (1984).
[7]A. D. Wieck, E. Batke, D. Heitmann, and J. P. Kotthous, Phys. Rev. B **30**, 4653 (1984).
[8]F. Martelli, C. Mazure, and F. Koch, Solid State Commun. **49**, 505 (1984).
[9]C. L. Yang, D. S. Pan, and R. Somoano, J. Appl. Phys. **65**, 3253 (1989).
[10]See H. J. Zeiger and G. W. Pratt, *Magnetic Interactions in Solids* (Clarendon, Oxford, 1973), Chap. 6, and references therein.
[11]K. S. Yi and J. J. Quinn, Phys. Rev. B **27**, 2396 (1983).
[12]J. M. Luttinger and W. Kohn, Phys. Rev. **97**, 869 (1955).
[13]F. Stern and W. E. Howard, Phys. Rev. **163**, 816 (1967).
[14]T. Ando, A. B. Fowler, and F. Stern, Rev. Mod. Phys. **54**, 437 (1982).
[15]J. J. Sakurai, *Modern Quantum Mechanics* (Benjamin/Cummings, Menlo Park, CA, 1985), Sec. 5.7.
[16]The second condition can be demonstrated easily if the quantum-well material is assumed to have a spherical conduction band. This leads to an expression for the transverse energy change, $\Delta\varepsilon_t=\hbar^2(\mathbf{k}_t+\boldsymbol{\beta}_t)^2/2m^*-\hbar^2\mathbf{k}_t^2/2m^*$, where $\mathbf{k}_t=k_x\mathbf{e}_x+k_y\mathbf{e}_y$, and similarly for $\boldsymbol{\beta}_t$. Thus, $\Delta\varepsilon_t=\hbar^2\mathbf{k}_t\cdot\boldsymbol{\beta}_t/m^*+\hbar^2\boldsymbol{\beta}_t^2/2m^*$, which is less than or equal to $\hbar\omega(v_t/c+\hbar\omega/2m^*c^2)$, where $v_t=\hbar|\mathbf{k}_t|/m^*$. In semiconductor quantum wells, $v_t$ is smaller than $c$, and $\hbar\omega$ is much less than the transverse rest-mass energy $m^*c^2$, so that $\Delta\varepsilon_t\ll\hbar\omega$.
[17]H. Lobentanzer, W. König, W. Stolz, K. Ploog, T. Elsaesser, and R. J. Bäuerle, Appl. Phys. Lett. **53**, 571 (1988).
[18]B. F. Levine, C. G. Bethea, K. K. Choi, J. Walker, and R. J. Malik, Appl. Phys. Lett. **53**, 231 (1988).
[19]The maximum absorption coefficient given in Ref. 18, $\cong 2.6\times10^3$ cm$^{-1}$, applies to a multiple-quantum-well structure including barrier regions. We divide this value by the fraction of the structure filled by quantum-well material to obtain $7.1\times10^3$ cm$^{-1}$.
[20]M. Neuberger, *Group IV Semiconducting Materials,* Vol. 5 of *Handbook of Electronic Materials* (Plenum, New York, 1971).
[21]H. C. Casey and M. B. Panish, *Heterostructure Lasers, Part B* (Academic, New York, 1978), Sec. 5.3.
[22]S. Adachi, J. Appl. Phys. **58**, R1 (1985).
[23]H. Hazama, Y. Itoh, and C. Hamaguchi, J. Phys. Soc. Jpn. **54**, 269 (1985).
[24]G. Hasnain, B. F. Levine, C. G. Bethea, R. A. Logan, J. Walker, and R. J. Malik, Appl. Phys. Lett. **54**, 2515 (1989).
[25]M. Fujimoto, J. Phys. Soc. Jpn. **21**, 1706 (1966).
[26]M. Neuberger, *III-V Semiconducting Compounds,* Vol. 2 of *Handbook of Electronic Materials* (Plenum, New York, 1971).